MATERIALS SCIENCE

Multidimensional coherent spectroscopy reveals triplet state coherences in cesium lead-halide perovskite nanocrystals

Albert Liu[1]*, Diogo B. Almeida[1]*, Luiz G. Bonato[2], Gabriel Nagamine[3], Luiz F. Zagonel[3], Ana F. Nogueira[2], Lazaro A. Padilha[3†], S. T. Cundiff[1†]

Advances in optoelectronics require materials with novel and engineered characteristics. A class of materials that has garnered tremendous interest is metal-halide perovskites, stimulated by meteoric increases in photovoltaic efficiencies of perovskite solar cells. In addition, recent advances have applied perovskite nanocrystals (NCs) in light-emitting devices. It was found recently that, for cesium lead-halide perovskite NCs, their unusually efficient light emission may be due to a unique excitonic fine structure composed of three bright triplet states that minimally interact with a proximal dark singlet state. To study this fine structure without isolating single NCs, we use multidimensional coherent spectroscopy at cryogenic temperatures to reveal coherences involving triplet states of a $CsPbI_3$ NC ensemble. Picosecond time scale dephasing times are measured for both triplet and inter-triplet coherences, from which we infer a unique exciton fine structure level ordering composed of a dark state energetically positioned within the bright triplet manifold.

INTRODUCTION

Cesium lead-halide perovskites were first synthesized over a century ago with a general chemical formula $CsPbX_3$ (where X = Cl, Br, or I). Recently, synthesis of $CsPbX_3$ nanocrystals (NCs) was achieved (*1*, *2*), which combines the advantages of perovskites (e.g., efficient luminescence and long carrier diffusion length) with those of colloidal NC materials (e.g., surface engineering and size-tunable emission). Perovskite NCs exhibit luminescence with quantum yields reaching nearly unity (*3*), in contrast to the optimized 80% quantum yield achieved by chalcogenide NCs coated with a gradient shell (*4*). Although all other colloidal materials suffer inhibited emission from lower-energy dark states (*5*), the unusual brightness of perovskite NCs is now believed to originate from an optically active, nondegenerate triplet state that emits efficiently despite the presence of a dark singlet state (*6*, *7*).

The unique exciton fine structure of perovskite NCs has substantially extended the potential applications of colloidal NCs. In particular, the three nondegenerate bright triplet states and their orthogonally oriented dipole moments (arising from atomic orbital mixing along the lattice symmetry axes) have generated much excitement for potential applications in quantum information processing (*8*, *9*). However, engineering exciton superposition states as information carriers will require an intimate knowledge of their coherent dynamics, which are still not well understood. The exciton fine structure of perovskite NCs has thus far only been studied via single-NC photoluminescence (*6*, *10*, *11*) and transient absorption (*12*, *13*) techniques, which have provided information only about their incoherent population dynamics. Furthermore, inhomogeneous spectral broadening due to NC size dispersion limits the utility of linear spectroscopic techniques in studying NC ensembles. More sophisticated methods are thus required (*14*–*17*) to extract the desired ensemble-averaged coherent properties of perovskite NCs.

Here, we extract crucial figures of merit for quantum information processing, the ensemble-averaged coherence times, and reveal coherence times of both optical triplet coherences and terahertz inter-triplet coherences for an ensemble of $CsPbI_3$ NCs (see Fig. 1, A and B) at cryogenic temperatures. We also present evidence for a mixed bright-dark level ordering (see Fig. 1C) that renders the triplet state excitons only partially bright. These measurements are enabled by using multidimensional coherent spectroscopy (MDCS) (*18*) to circumvent the inhomogeneous broadening that obscures spectral signatures of the exciton fine structure and resolve coherent coupling involving different triplet states. The extracted coherence times for $CsPbI_3$ NCs are an order of magnitude longer compared to candidate materials for valleytronics (*14*, *15*, *19*), which positions perovskite NCs as a potential material platform for quantum information applications via bottom-up assembly.

RESULTS

Multidimensional coherent spectroscopy

To perform MDCS, we use a multidimensional optical nonlinear spectrometer (*20*), which focuses three laser pulses onto the perovskite NC ensemble sample as a function of three time delays τ, T, and t (schematically shown in Fig. 1, C and D). By Fourier transforming the emitted four-wave mixing (FWM) signal as a function of two or all three time delays, the coherences and populations induced by each pulse are correlated in a multidimensional spectrum. In order, the first pulse (A) generates a coherent superposition between the ground and an optically active excited state, which oscillates at the energy difference $\hbar\omega_\tau$. The second pulse (B) then converts this optical coherence into either a population state that decays according to its relaxation rate or a coherence between two neighboring states within a ground or excited state manifold that oscillates at $\hbar\omega_T$. The last pulse (C) then generates a final optical coherence that oscillates at $\hbar\omega_t$ and radiates an FWM signal. These sequences of light-matter interactions are commonly referred to as quantum pathways [(*21*)

[1]Department of Physics, University of Michigan, Ann Arbor, MI 48109, USA. [2]Instituto de Química, Universidade Estadual de Campinas, 13083-970 Campinas, São Paulo, Brazil. [3]Instituto de Física "Gleb Wataghin," Universidade Estadual de Campinas, 13083-970 Campinas, São Paulo, Brazil.
*These authors contributed equally to this work.
†Corresponding author. Email: padilha@ifi.unicamp.br (L.A.P.); cundiff@umich.edu (S.T.C.)

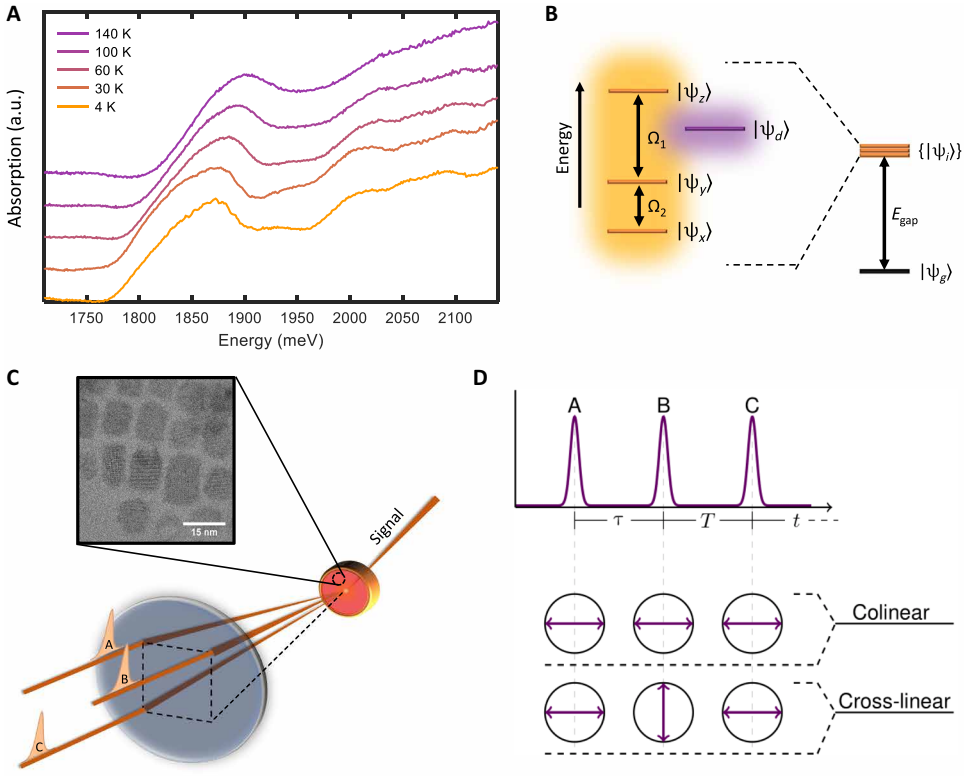

Fig. 1. $CsPbI_3$ perovskite NCs studied via MDCS. (**A**) Perovskite NC absorption spectra as a function of temperature (*34*). (**B**) Energy level diagram of the nondegenerate bright triplet states $\{\Psi_{i=x,y,z}\}$ that comprise the band-edge transitions to and from $|\Psi_g\rangle$. The dark singlet state $|\Psi_d\rangle$ is shown to lie between states $|\Psi_y\rangle$ and $|\Psi_z\rangle$, which is argued in the main text. (**C**) Schematic of the MDCS experiment. Three pulses {A,B,C} are focused onto the sample with varying time delays. Inset shows a transmission electron micrograph of representative $CsPbI_3$ NCs. (**D**) Excitation pulse sequence and excitation polarization schemes used to acquire one-quantum and zero-quantum spectra, in which double-sided arrows in circles denote the polarization of each pulse. Pulses A and C are horizontally polarized, and pulse B is either horizontally or vertically polarized, which corresponds to an emitted signal of either horizontal or vertical polarization respectively. a.u., arbitrary units.

and the Supplementary Materials]. Fourier transforming along the variables τ and t returns one-quantum spectra (which correlate the absorption energy $\hbar\omega_\tau$ with the emission energy $\hbar\omega_t$) and has been applied in recent studies (*22*–*24*) to reveal novel electronic properties of various perovskite materials. In this study, we also transform along the variables T and t to obtain zero-quantum spectra [which correlate the intraband mixing energy (*25*) $\hbar\omega_T$ and the emission energy $\hbar\omega_t$]. Furthermore, the polarization of the second pulse is chosen to align either parallel or orthogonal to the colinear polarizations of the other two pulses to probe different quantum pathways. We denote the two polarization schemes as colinear excitation and cross-linear excitation, respectively, as shown in Fig. 1D.

One-quantum spectra probe optical triplet coherences

One-quantum spectra were acquired at a temperature of 4.6 K with colinear and cross-linear excitation (shown in Fig. 2, A and B). Both spectra reveal numerous peaks elongated in the diagonal direction ($|\hbar\omega_\tau| = |\hbar\omega_t|$), reflecting inhomogeneous spectral broadening (*26*). Cross-slices taken in the orthogonal direction, which reflect the ensemble-averaged homogeneous response at a certain resonance energy (*26*), are plotted in Fig. 2 (C and D). In the full slices (inset), asymmetric peaks are observed for $|\Delta E| > 4$ meV, which could arise from either electron-phonon coupling (*27*) or biexciton transitions (*28*). Here, we focus on features related to the triplet state fine structure and defer discussion of vibrational features and biexciton transitions [which appear at the biexciton binding energy $\Delta E = -E_{XX}$, which is well over 10 meV (*10*), and do not influence the low-energy features studied here] to future reports. The main plots of each slice section (highlighted by the yellow boxes inset) show symmetric peaks that, due to their polarization dependence, we attribute to absorption and emission involving different triplet state coherences. As described above, the origin of the observed peaks is interpreted as changes in the system density matrix induced by each pulse that form accessible quantum pathways (*21*). First, peaks 1 and 3 in Fig. 2C are generated by absorption and emission of coherences involving $|g\rangle$ and both triplet states $|\Psi_x\rangle$ and $|\Psi_y\rangle$. We note that our measurements do not inform the ordering of states $|\Psi_{x/y}\rangle$, so we assume the ordering shown in Fig. 1B for labeling the dephasing rates discussed below. The central peak 2 is likewise generated by quantum pathways involving absorption and emission by coherences of identical resonance energy $|g\rangle\langle\Psi_i|$ and $|\Psi_i\rangle\langle g|$, respectively. In Fig. 2D, peaks 1 and 3 are visible as shoulders on two new peaks 4 and 5, which are generated by absorption and emission of coherences involving $|g\rangle$ and triplet states $|\Psi_y\rangle$ and $|\Psi_z\rangle$.

The polarization dependences of the five observed peaks is not immediately intuitive. To explain the peak structure for both excitation polarization schemes, we theoretically calculate the relative peak strengths for varying dipole matrix elements and vector orientations of each triplet state transition (see the Supplementary Materials). From these calculations, we draw two important conclusions: (i) To observe sidebands

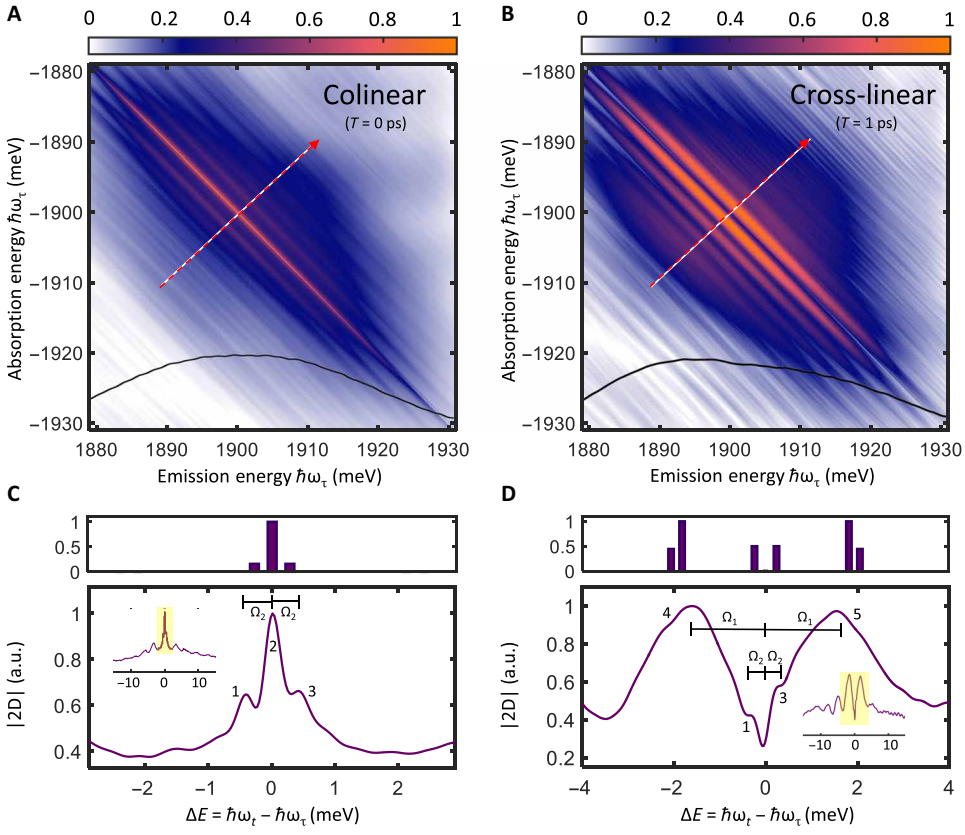

Fig. 2. Optical triplet coherences in one-quantum spectra. (**A** and **B**) Magnitude one-quantum spectrum at 4.6 K with (A) colinear and (B) cross-linear excitation. The white/red dashed arrows and solid black lines indicate the cross-slice locations and laser pulse spectra, respectively. (**C** and **D**) Bottom plots show normalized cross-slices centered at $|\hbar\omega_\tau| = |\hbar\omega_t| = 1900$ meV of the (C) colinear and (D) cross-linear excitation one-quantum spectrum. Top plots show theoretically calculated relative peak strengths in the NC reference frame (see the Supplementary Materials). Numbers label peaks arising from electronic interband coherences and populations.

with colinear excitation, the two triplet states involved must have transition dipole moments that are not perpendicular, and (ii) for peaks 4 and 5 to each be primarily composed of a single peak located at $\Delta E = \pm\Omega_1$, as suggested by our fitting attempts, the dipole moment of $|\Psi_y\rangle$ must be substantially stronger than those of $|\Psi_x\rangle$ and $|\Psi_z\rangle$. We achieve good agreement with experiment for a 45° angle between the dipole moments of $|\Psi_x\rangle$ and $|\Psi_y\rangle$ and a dipole matrix element of $|\Psi_y\rangle$ that is 1.5 times the magnitude of the dipole matrix elements of $|\Psi_x\rangle$ and $|\Psi_z\rangle$ (see the Supplementary Materials).

Fitting the cross-diagonal line shapes also extracts the homogeneous linewidths γ_i (*25*) of triplet state transitions between $|g\rangle$ and $|\Psi_i\rangle$. In this context, one-quantum spectra are particularly useful when compared to integrated FWM techniques (*29*), since the cross-diagonal slice position $|\hbar\omega_\tau| = |\hbar\omega_t|$ reflects an effective NC size (see the Supplementary Materials). Although peaks 1 and 4 and peaks 3 and 5 would ideally be mirror images, vibrational coupling distorts the line shapes of peaks 1 and 4. We thus fit only the $\Delta E \geq 0$ side (details are in the Supplementary Materials). Fit of the colinear slice line shape (Fig. 2C) gives a sideband (peaks 1 and 3) dephasing rate $\hbar\frac{\gamma_x+\gamma_y}{2} = 0.120 \pm 0.023$ meV (5.49 ps) and a zero-phonon line (peak 2) dephasing rate of 0.124 ± 0.008 meV (5.32 ps). Fit of peaks 4 and 5 in the cross-linear slice line shape (Fig. 2D) gives a dephasing rate $\hbar\frac{\gamma_y+\gamma_z}{2} = 0.496 \pm 0.017$ meV (1.33 ps). The fitted triplet state energy splittings are likewise $\Omega_1 = 1.82 \pm 0.02$ meV and $\Omega_2 = 0.24 \pm 0.016$ meV. The provided parameter uncertainties reflect the accuracy of the fitting procedure rather than statistical error. If the dipole moment of state $|\Psi_y\rangle$ is indeed much larger than those of $|\Psi_x\rangle$ and $|\Psi_z\rangle$, the zero-phonon line dephasing rate will approximately equal $\hbar\gamma_y$, which, in turn, determines the individual triplet state dephasing rates $\gamma_x = 0.116$ meV ($T_2^x = 5.68$ ps), $\gamma_y = 0.124$ meV ($T_2^y = 5.32$ ps), and $\gamma_z = 0.868$ meV ($T_2^z = 0.76$ ps). To test the above claim, fits assuming additional peaks at $\Delta E = \pm(\Omega_1 + \Omega_2)$ were attempted but did not yield reasonable line shapes.

Zero-quantum spectra probe terahertz inter-triplet coherences

Many of the quantum pathways that generate the sidebands in Fig. 2 (A and B) involve inter-triplet coherences, which are quantum coherences between triplet states that are not necessarily dipole-coupled (*30*). Of both fundamental and practical importance is the inter-triplet coherence time, which defines the time scale during which the superposition states involved may be coherently manipulated. Inter-triplet coherences are those density matrix elements of the form $|\Psi_i\rangle\langle\Psi_j|$ where $i, j = \{x,y,z\}$ and $i \neq j$. To directly measure and characterize these coherences, we take zero-quantum spectra at varying temperature and delay τ. For colinear excitation, no inter-triplet coherences between $|\Psi_x\rangle$ and $|\Psi_y\rangle$ are observed (see the Supplementary Materials). It is ambiguous whether their corresponding peaks are weak or are simply obscured by the linewidth of a central $\hbar\omega_T = 0$ peak. For cross-linear excitation, we further isolate the inter-triplet

coherence pathways by passing the measured FWM signal through a vertical polarizer. We plot a resultant cross-linear zero-quantum spectrum at 20 K in Fig. 3A. Sidebands are observed at mixing energies identical to the positions of peaks 4 and 5 in Fig. 2D, which we attribute to inter-triplet coherences between $|\Psi_y\rangle$ and $|\Psi_z\rangle$. An inter-triplet coherence between $|\Psi_x\rangle$ and $|\Psi_z\rangle$ is observed in neither the colinear nor cross-linear zero-quantum spectra, which is consistent with a dominant transition dipole of state $|\Psi_y\rangle$ as argued above.

In Fig. 3B, the evolutions of normalized slices (at $\hbar\omega_T = 1890$ meV) as a function of delay τ and temperature are shown. The FWM signal dephases rapidly with increasing τ and results in an equally rapid decrease of sideband visibility (see the Supplementary Materials), in contrast to the opposite behavior of vibrational intraband coherences [see (*16*) and the Supplementary Materials], which confirms its electronic nature. No change in the amplitude ratio between sidebands 6 and 8 is observed as temperature increases, confirming that the state splitting observed indeed belongs to the bright triplet excited state rather than from thermal filling of higher-lying ground states. We note that the triplet state coherences in one-quantum spectra broaden substantially with increasing temperature and are not resolved at temperatures above 15 K. In contrast, minimal broadening of the inter-triplet coherence linewidth is observed up to 40 K (see Fig. 3B), indicating that inter-triplet coherences are robust against thermal dephasing (*14*).

A slice at $\tau = 0$ fs is plotted in Fig. 3C, from which we can extract the inter-triplet coherence time. However, the quantum pathways that generate peaks 6 and 8 involve identical dipole moments $\mu_y^2\mu_z^2$, from which we expect equal peak amplitudes contrary to the uneven peaks observed. This difference is due to interference between the three complex Lorentzian line shapes underlying the overall amplitude line shape (see the Supplementary Materials), and the fit to experiment is performed by shifting the phase of each sideband Lorentzian line shape by identical factors of $-\pi/2$ relative to the central $\hbar\omega_T = 0$ peak. These phase factors arise from a $-\pi/4$ phase difference between the complex transition dipole moments μ_y and μ_z, which may be directly related to structural information about the initial/final states of an optical transition and their associated wave functions (*31*). From our fit, we extract an energy splitting $\Omega_1 = 1.61$ meV and an inter-triplet coherence time $T_2^{yz} = 1.36$ ps at 20 K.

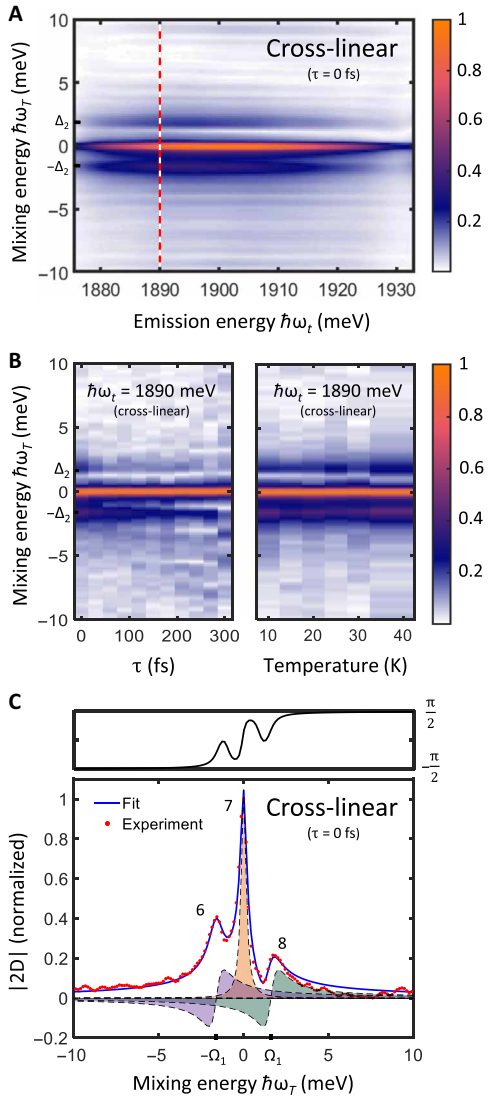

Fig. 3. Terahertz inter-triplet coherences in zero-quantum spectra. (**A**) Magnitude zero-quantum spectrum taken at $\tau = 0$ fs and 20 K. Two sidebands due to inter-triplet coherences are observed. (**B**) Evolution of normalized slices taken along the dashed red line in (A) at $\hbar\omega_\tau = 1890$ meV as a function of delay τ (at 20 K) and temperatures [10, 15, 20, 25, 30, 40] K (at $\tau = 0$ fs). (**C**) Fit of normalized cross-slice taken at $\tau = 0$ fs, in which the complex Lorentzians of peaks 6 and 8 are shifted by phases $-\pi/2$ relative to peak 7. The shaded curves represent the real quadratures of each Lorentzian in the fit line shape, and the top plot is the phase of the fitted complex line shape.

DISCUSSION

It is quite unexpected that the optical dephasing rate γ_z is so much faster than those of the other two triplet states γ_x and γ_y. Although this disparity suggests a fundamentally different dephasing mechanism for coherences involving state $|\Psi_z\rangle$, photoluminescence of similar orthorhombic perovskite NCs that exhibit triplet state structure reveals similar emission linewidths for all three states of the manifold (*6*, *7*). We resolve this discrepancy by proposing a unique exciton fine structure composed of a dark singlet state $|\Psi_d\rangle$ that lies above the states $|\Psi_x\rangle$ and $|\Psi_y\rangle$, which form the band edge, while remaining below the third triplet state $|\Psi_z\rangle$ (shown in Fig. 1B). Camargo *et al.* (*24*) have similarly applied MDCS to reveal dark states in a perovskite thin film, although the sub-gap defect states they observe are fundamentally different from the dark state discussed here, which arises from the lead-halide atomic orbitals and would exist in a perfect lattice. For our proposed level ordering, rapid relaxation from $|\Psi_z\rangle$ to $|\Psi_d\rangle$ then significantly decreases the population lifetime T_1^z and consequently T_2^z as well (*21*). Such a fine structure has been theoretically predicted in certain ranges of NC size due to competition between the Rashba effect and electron-hole exchange interaction (*32*). Although we cannot rule out alternative sources of line broadening, such as the imperfect correlation between the two inhomogeneously broadened transitions between the ground state and $\{|\Psi_y\rangle, |\Psi_z\rangle\}$ that would selectively broaden sidebands 4 and 5 in Fig. 2 (see the Supplementary Materials), our hypothesis is further supported by previous photoluminescence studies of $CsPbI_3$ NCs of nearly identical size (*10*). These incoherent spectra, which are not affected by inhomogeneous broadening correlation, revealed polarized doublets corresponding to $|\Psi_x\rangle$ and $|\Psi_y\rangle$ but did not detect the third triplet

state $|\Psi_z\rangle$ (whose emission would be quenched by nonradiative relaxation to $|\Psi_d\rangle$ according to our hypothesis of a partially bright triplet exciton band edge). In accordance with the predicted size dependence of the relative dark state energy (*32*), we also observe an abrupt increase in T_2^y with increasing slice position (see the Supplementary Materials), which results from a crossing in energy of $|\Psi_y\rangle$ and $|\Psi_d\rangle$. These results stand in stark contrast to recent studies of $CsPbBr_2Cl$ (*6*) and $FAPbBr_3$ (*7*) NCs, which have reported the highest- and lowest-lying dark states, respectively. Evidently, a change in even a single constituent atom of the perovskite lattice may drastically alter the exchange and Rashba interaction coefficient ratio that determines the fine structure level ordering (*32*), which warrants future investigation.

To conclude, we have measured and characterized both optical frequency triplet coherences and terahertz frequency inter-triplet coherences. We have also presented evidence of an exciton band edge whose emission is partially quenched by an intermediate dark state, which contributes important insight into the controversial nature of exciton ground states in different perovskite NC materials (*6*, *7*). As a material still in its infancy, perovskite NCs show promise for applications in optoelectronic devices. In particular, the minimal thermal broadening of inter-triplet coherences observed here motivates study of applications above cryogenic temperatures. For example, in a triplet state analog of valleytronics in two-dimensional materials (*19*), superpositions of triplet states could be initialized and read out with linearly polarized light and coherently manipulated via terahertz radiation as information carriers (*33*).

MATERIALS AND METHODS

The NCs studied are cube-shaped, with side lengths of 8.7 ± 2.6 nm measured from 100 NCs in transmission electron microscopy measurements. These sizes are comparable to the $CsPbI_3$ exciton Bohr diameter (12 nm) and correspond to a room temperature 1S exciton absorption peak centered around 1900 meV (shown in Fig. 1B). The synthesis method is described in the Supplementary Materials. To study these NCs using MDCS at cryogenic temperatures, we disperse them in heptamethylnonane and load the colloidal suspension in a copper sample holder with 0.5-mm-thick sapphire windows. The sample optical density is measured to be 0.3 at room temperature 1S exciton absorption peak. Upon cooling of the sample below ~100 K, heptamethylnonane freezes into a transparent glass, resulting in a stationary, randomly oriented NC ensemble.

To perform MDCS, we use a multidimensional optical nonlinear spectrometer (*20*), which focuses three laser pulses onto the sample. The excitation pulses are of 90 fs duration at a 250-kHz repetition rate, and the excitation intensity of 5 W/cm^2 generates a predominately third-order response as verified by a power-dependence measurement of the generated transient FWM signal. The emitted signal is then heterodyne-detected with a co-propagating local-oscillator pulse as a function of time delays τ, *T*, and/or *t* with sub-wavelength stability.

SUPPLEMENTARY MATERIALS

Supplementary material for this article is available at http://advances.sciencemag.org/cgi/content/full/7/1/eabb3594/DC1

REFERENCES AND NOTES

1. L. Protesescu, S. Yakunin, M. I. Bodnarchuk, F. Krieg, R. Caputo, C. H. Hendon, R. X. Yang, A. Walsh, M. V. Kovalenko, Nanocrystals of cesium lead halide perovskites ($CsPbX_3$, X = Cl, Br, and I): Novel optoelectronic materials showing bright emission with wide color gamut. *Nano Lett.* **15**, 3692–3696 (2015).
2. S.-T. Ha, R. Su, J. Xing, Q. Zhang, Q. Xiong, Metal halide perovskite nanomaterials: Synthesis and applications. *Chem. Sci.* **8**, 2522–2536 (2017).
3. F. Liu, Y. Zhang, C. Ding, S. Kobayashi, T. Izuishi, N. Nakazawa, T. Toyoda, T. Ohta, S. Hayase, T. Minemoto, K. Yoshino, S. Dai, Q. Shen, Highly luminescent phase-stable CsPbI3 perovskite quantum dots achieving near 100% absolute photoluminescence quantum yield. *ACS Nano* **11**, 10373–10383 (2017).
4. J. Lim, B. G. Jeong, M. Park, J. K. Kim, J. M. Pietryga, Y.-S. Park, V. I. Klimov, C. Lee, D. C. Lee, W. K. Bae, Influence of shell thickness on the performance of light-emitting devices based on CdSe/$Zn_{1-X}Cd_XS$ core/shell heterostructured quantum dots. *Adv. Mater.* **26**, 8034–8040 (2014).
5. M. Nirmal, D. J. Norris, M. Kuno, M. G. Bawendi, A. L. Efros, M. Rosen, Observation of the "dark exciton" in CdSe quantum dots. *Phys. Rev. Lett.* **75**, 3728–3731 (1995).
6. M. A. Becker, R. Vaxenburg, G. Nedelcu, P. C. Sercel, A. Shabaev, M. J. Mehl, J. G. Michopoulos, S. G. Lambrakos, N. Bernstein, J. L. Lyons, T. Stöferle, R. F. Mahrt, M. V. Kovalenko, D. J. Norris, G. Rainò, A. L. Efros, Bright triplet excitons in caesium lead halide perovskites. *Nature* **553**, 189–193 (2018).
7. P. Tamarat, M. I. Bodnarchuk, J.-B. Trebbia, R. Erni, M. V. Kovalenko, J. Even, B. Lounis, The ground exciton state of formamidinium lead bromide perovskite nanocrystals is a singlet dark state. *Nat. Mater.* **18**, 717–724 (2019).
8. G. Rainò, M. A. Becker, M. I. Bodnarchuk, R. F. Mahrt, M. V. Kovalenko, T. Stöferle, Superfluorescence from lead halide perovskite quantum dot superlattices. *Nature* **563**, 671–675 (2018).
9. H. Utzat, W. Sun, A. E. K. Kaplan, F. Krieg, M. Ginterseder, B. Spokoyny, N. D. Klein, K. E. Shulenberger, C. F. Perkinson, M. V. Kovalenko, M. G. Bawendi, Coherent single-photon emission from colloidal lead halide perovskite quantum dots. *Science* **363**, 1068–1072 (2019).
10. C. Yin, L. Chen, N. Song, Y. Lv, F. Hu, C. Sun, W. W. Yu, C. Zhang, X. Wang, Y. Zhang, M. Xiao, Bright-exciton fine-structure splittings in single perovskite nanocrystals. *Phys. Rev. Lett.* **119**, 026401 (2017).
11. L. Chen, B. Li, C. Zhang, X. Huang, X. Wang, M. Xiao, Composition-dependent energy splitting between bright and dark excitons in lead halide perovskite nanocrystals. *Nano Lett.* **18**, 2074–2080 (2018).
12. N. S. Makarov, S. Guo, O. Isaienko, W. Liu, I. Robel, V. I. Klimov, Spectral and dynamical properties of single excitons, biexcitons, and trions in cesium-lead-halide perovskite quantum dots. *Nano Lett.* **16**, 2349–2362 (2016).
13. J. A. Castañeda, G. Nagamine, E. Yassitepe, L. G. Bonato, O. Voznyy, S. Hoogland, A. F. Nogueira, E. H. Sargent, C. H. Brito Cruz, L. A. Padilha, Efficient biexciton interaction in perovskite quantum dots under weak and strong confinement. *ACS Nano* **10**, 8603–8609 (2016).
14. G. Moody, C. K. Dass, K. Hao, C.-H. Chen, L.-J. Li, A. Singh, K. Tran, G. Clark, X. Xu, G. Berghäuser, E. Malic, A. Knorr, X. Li, Intrinsic homogeneous linewidth and broadening mechanisms of excitons in monolayer transition metal dichalcogenides. *Nat. Commun.* **6**, 8315 (2015).
15. K. Hao, G. Moody, F. Wu, C. K. Dass, L. Xu, C.-H. Chen, L. Sun, M.-Y. Li, L.-J. Li, A. H. Mac Donald, X. Li, Direct measurement of exciton valley coherence in monolayer WSe_2. *Nat. Phys.* **12**, 677–682 (2016).
16. A. Liu, D. B. Almeida, W. K. Bae, L. A. Padilha, S. T. Cundiff, Non-markovian exciton-phonon interactions in core-shell colloidal quantum dots at femtosecond timescales. *Phys. Rev. Lett.* **123**, 057403 (2019).
17. A. Liu, D. B. Almeida, W.-K. Bae, L. A. Padilha, S. T. Cundiff, Simultaneous existence of confined and delocalized vibrational modes in colloidal quantum dots. *J. Phys. Chem. Lett.* **10**, 6144–6150 (2019).
18. S. T. Cundiff, S. Mukamel, Optical multidimensional coherent spectroscopy. *Phys. Today* **66**, 44–49 (2013).
19. J. R. Schaibley, H. Yu, G. Clark, P. Rivera, J. S. Ross, K. L. Seyler, W. Yao, X. Xu, Valleytronics in 2D materials. *Nat. Rev. Mater.* **1**, 16055 (2016).
20. A. D. Bristow, D. Karaiskaj, X. Dai, T. Zhang, C. Carlsson, K. R. Hagen, R. Jimenez, S. T. Cundiff, A versatile ultrastable platform for optical multidimensional Fourier-transform spectroscopy. *Rev. Sci. Instrum.* **80**, 073108 (2009).
21. S. Mukamel, *Principles of Nonlinear Optical Spectroscopy* (Oxford Univ. Press, ed. 1, 1999).
22. H. Seiler, S. Palato, C. Sonnichsen, H. Baker, E. Socie, D. P. Strandell, P. Kambhampati, Two-dimensional electronic spectroscopy reveals liquid-like lineshape dynamics in $CsPbI_3$ perovskite nanocrystals. *Nat. Commun.* **10**, 4962 (2019).
23. W. Zhao, Z. Qin, C. Zhang, G. Wang, X. Huang, B. Li, X. Dai, M. Xiao, Optical gain from biexcitons in $CsPbBr_3$ nanocrystals revealed by two-dimensional electronic spectroscopy. *J. Phys. Chem. Lett.* **10**, 1251–1258 (2019).
24. F. V. A. Camargo, T. Nagahara, S. Feldmann, J. M. Richter, R. H. Friend, G. Cerullo, F. Deschler, Dark subgap states in metal-halide perovskites revealed by coherent multidimensional spectroscopy. *J. Am. Chem. Soc.* **142**, 777–782 (2020).
25. L. Yang, T. Zhang, A. D. Bristow, S. T. Cundiff, S. Mukamel, Isolating excitonic Raman coherence in semiconductors using two-dimensional correlation spectroscopy. *J. Chem. Phys.* **129**, 234711 (2008).

26. M. E. Siemens, G. Moody, H. Li, A. D. Bristow, S. T. Cundiff, Resonance lineshapes in two-dimensional Fourier transform spectroscopy. *Opt. Express* **18**, 17699–17708 (2010).
27. A. Liu, S. T. Cundiff, Spectroscopic signatures of electron-phonon coupling in silicon-vacancy centers in diamond. *Phys. Rev. Mater.* **4**, 055202 (2020).
28. K. Hao, J. F. Specht, P. Nagler, L. Xu, K. Tran, A. Singh, C. K. Dass, C. Schüller, T. Korn, M. Richter, A. Knorr, X. Li, G. Moody, Neutral and charged inter-valley biexcitons in monolayer $MoSe_2$. *Nat. Commun.* **8**, 15552 (2017).
29. M. A. Becker, L. Scarpelli, G. Nedelcu, G. Rainò, F. Masia, P. Borri, T. Stöferle, M. V. Kovalenko, W. Langbein, R. F. Mahrt, Long exciton dephasing time and coherent phonon coupling in $CsPbBr_2Cl$ perovskite nanocrystals. *Nano Lett.* **18**, 7546–7551 (2018).
30. K. B. Ferrio, D. G. Steel, Raman quantum beats of interacting excitons. *Phys. Rev. Lett.* **80**, 786–789 (1998).
31. S. Haessler, J. Caillat, W. Boutu, C. Giovanetti-Teixeira, T. Ruchon, T. Auguste, Z. Diveki, P. Breger, A. Maquet, B. Carré, R. Taïeb, P. Salières, Attosecond imaging of molecular electronic wavepackets. *Nat. Phys.* **6**, 200–206 (2010).
32. P. C. Sercel, J. L. Lyons, D. Wickramaratne, R. Vaxenburg, N. Bernstein, A. L. Efros, Exciton fine structure in perovskite nanocrystals. *Nano Lett.* **19**, 4068–4077 (2019).
33. F. Langer, C. P. Schmid, S. Schlauderer, M. Gmitra, J. Fabian, P. Nagler, C. Schüller, T. Korn, P. G. Hawkins, J. T. Steiner, U. Huttner, S. W. Koch, M. Kira, R. Huber, Lightwave valleytronics in a monolayer of tungsten diselenide. *Nature* **557**, 76–80 (2018).
34. A. Liu, L. G. Bonato, F. Sessa, D. B. Almeida, E. Isele, G. Nagamine, L. F. Zagonel, A. F. Nogueira, L. A. Padilha, S. T. Cundiff, Effect of dimensionality on the optical absorption properties of $CsPbI_3$ perovskite nanocrystals. *J. Chem. Phys.* **151**, 191103 (2019).
35. G. Scholes, Selection rules for probing biexcitons and electron spin transitions in isotropic quantum dot ensembles. *J. Chem. Phys.* **121**, 10104–10110 (2004).
36. S. T. Cundiff, Effects of correlation between inhomogeneously broadened transitions on quantum beats in transient four-wave mixing. *Phys. Rev. A* **49**, 3114–3118 (1994).

Acknowledgments

Funding: This work was supported by the Department of Energy grant number DE-SC0015782. D.B.A. acknowledges support from the Brazilian National Council for Scientific and Technological Development (CNPq). L.A.P. acknowledges support from FAPESP (project numbers 2013/16911-2 and 2016/50011-7). Research was also supported by LNNano/CNPEM/MCTIC, where the transmission electron microscopy measurements were performed. **Author contributions:** L.A.P. and S.T.C. conceived the concept. Supervised by A.F.N., L.G.B. synthesized the perovskite NC sample. G.N. and L.F.Z. acquired transmission electron microscopy images of the sample and characterized the NC size. A.L. and D.B.A. ran the experiments and acquired the data. A.L. analyzed the results and wrote the manuscript. All authors discussed the results and commented on the manuscript at all stages. **Competing interests:** The authors declare that they have no competing interests. **Data and materials availability:** All data needed to evaluate the conclusions in the paper are present in the paper and/or the Supplementary Materials. Additional data related to this paper may be requested from the authors.

Submitted 18 February 2020
Accepted 10 November 2020
Published 1 January 2021
10.1126/sciadv.abb3594

Citation: A. Liu, D. B. Almeida, L. G. Bonato, G. Nagamine, L. F. Zagonel, A. F. Nogueira, L. A. Padilha, S. T. Cundiff, Multidimensional coherent spectroscopy reveals triplet state coherences in cesium lead-halide perovskite nanocrystals. *Sci. Adv.* **7**, eabb3594 (2021).